Parametric Optimization Erosion Wear of Polyester-GF-Alumina Hybrid Composites using the Taguchi Method

First published on February 25, 2008

Journal of Reinforced Plastics and Composites 2008

http://dx.doi.org/10.1177/0731684407086867

Parametric Optimization Erosion Wear of Polyester-GF-Alumina Hybrid Composites using the Taguchi Method

AMAR PATNAIK*
Department of Mechanical Engineering, National Institute of Technology Hamirpur – 177005, India

ALOK SATATPATHY AND S. S. MAHAPATRA
Department of Mechanical Engineering, National Institute of Technology Rourkela – 769008, India

R. R. DASH
Department of Mechanical Engineering, G.I.E.T, Gunupur – 765022, India

ABSTRACT: The improved performance of polymer-based hybrid composites in tribological applications has recently been a subject of considerable interest. A hybrid composite consists of the matrix reinforced with both fibers and particulate fillers. Alumina has the potential to be used as filler in such a multi-component system. This article investigates the effect of alumina filling on the erosion wear performance of glass fiber-reinforced polyester composites. For this purpose, an air jet type erosion test configuration and the design of experiment approach utilizing Taguchi's orthogonal arrays are used. Taguchi's design eliminates the need for repeated experiments; thus saving time, materials, and cost. The systematic experimentation leads to identifying significant factors and their interactions that predominantly influence the erosion wear. Pure glass-polyester composite without filler shows greater erosion rate whereas a significant improvement in the erosion resistance is observed with alumina fillers. This may be due to restriction of fiber-matrix debonding. The morphologies of the eroded surface are examined by a scanning electron microscope. Finally, optimal factor settings for minimum wear rate have been determined using genetic algorithm.

KEY WORDS: polymer matrix composites, wear, micro-structure, Taguchi method.

INTRODUCTION

MAJOR NEW APPLICATIONS in aeronautics, automobiles, power generation, and petroleum industries using polymer composites are springing up at an ever-increasing pace. In these appliations, fiber-reinforced polymers have to function in severe erosive environments and this often leads to their failure. Hard particulate fillers, consisting of ceramic or metal particles, and fiber fillers made of glass are being used these days to dramatically improve the wear resistance, even up to three orders of magnitude [1]. The improved performance of polymers and their composites in tribological applications by

*Author to whom correspondence should be addressed. E-mail: amar_mecha@yahoo.co.uk

the addition of filler materials has shown great promise and so has lately been a subject of considerable interest. The filler materials include organic, inorganic, and metallic particulate materials in both micro and nano sizes. Various kinds of polymers and polymer-matrix composites reinforced with metal particles have a wide range of industrial applications, such as heaters, electrodes [2], composites with thermal durability at high temperature [3], etc. These engineering composites are desired due to their low density, high corrosion resistance, ease of fabrication, and low cost [4–6]. Similarly, ceramic-filled polymer composites have been the subject of extensive research in the last two decades. The inclusion of inorganic fillers into polymers for commercial applications is primarily aimed at the cost reduction and stiffness improvement [7,8]. Along with fiber-reinforced composites, the composites made with particulate fillers have been found to perform well in tribological conditions.

Erosive wear of engineering components caused by abrasive particles is a major industrial problem. A full understanding of the effects of all system variables on the wear rate is necessary in order to undertake appropriate steps in the design of machine or structural component and in the choice of materials to reduce/control wear. In recent years much research has been devoted to exploring the potential advantages of thermoplastic polymers for composite materials. Some of the commonly used thermoplastics are polyetheretherketone (PEEK), polyetherketone (PEK), polyetherketoneketone (PEKK), polyester, polypropylene (PP), etc. Several investigations on friction and wear properties of PEEK and its composites filled with fibers, organic, and inorganic fillers have been carried out [9,18]. Cirino et al. [9,10] reported the sliding, as well as the abrasive wear behavior, of continuous carbon and aramid fiber-reinforced PEEK. Lhymn et al. [11] have studied the abrasive wear of short carbon fiber-reinforced PEEK. Voss and Friedrich [12] investigated the sliding and abrasive wear behavior of short fiber-reinforced PEEK composites at room temperature. Briscoe et al. [13] described the friction and wear of PEEK-PTFE blends over a wide composition range under several testing conditions. Friedrich et al. [14] investigated the sliding and abrasive wear behavior of short fiber-reinforced PEEK composites at room temperature. Bahadur and Gong [15] investigated the action of various copper compounds as fillers on the tribological behavior of PEEK. Wang et al. [16–18] investigated friction and wear properties of nanometric ZrO_2 and SiC-filled PEEK composites with different filler proportions. Most of the above studies are confined to dry sliding of PEEK and its composites. The erosive wear behavior of polyester composites reinforced with any fiber or particulate has not yet been reported in the literature. In view of the above, the objective of the present investigation is to study the effect of glass fiber reinforcement and inclusion of alumina filler on the erosive wear behavior of polyester under multiple impact conditions.

Alumina is one such inorganic material that has the potential to be used as filler in various polymer matrices. Aluminum oxide (Al_2O_3), commonly referred to as alumina, can exist in several crystalline phases, all of which revert to the most stable hexagonal alpha phase at elevated temperatures. This is the phase of particular interest for structural applications. Alumina is the most cost effective and widely used material in the family of engineering ceramics. It is hard, wear resistant, has excellent dielectric properties, resistance to strong acid and alkali attack at elevated temperatures, high strength, and stiffness. With an excellent combination of properties and a reasonable price, it is no surprise that fine grain technical grade alumina has a very wide range of applications.

To obtain the desired properties, reinforcement and fillers are added to the polymers. The additional improvements in mechanical and tribological properties are in many cases attained through the incorporation of glass or carbon fiber reinforcement. However, tribo

properties are not intrinsic material properties, but strongly depend upon the system in which the material functions [19]. So the influence of fillers and fibers on the tribo-behavior of composites cannot be predicted *a priori* and has to be tested in the laboratory. In many industrial applications of composites, an understanding of tribological behavior is necessary along with an understanding of the mechanical properties [20]. Hence, the primary concern here is to study how the alumina particle-filled glass fiber-reinforced polyester composites respond to the impact of erodent particles under different operating conditions, to assess the damage due to wear, and finally to determine the optimal parameter settings for minimum wear loss.

EXPERIMENTAL

Specimen Preparation

E-glass fibers (360 roving taken from Saint Govion) are reinforced in alumina-filled unsaturated isophthalic polyester resin to prepare hybrid composites. The composite slabs are prepared by conventional hand-lay up technique. Two percent (2%) cobalt nephthalate (as accelerator) is mixed thoroughly in isophthalic polyester resin and then 2% methyl-ethyl-ketone-peroxide (MEKP) as hardener is mixed in the resin prior to reinforcement. The filler material alumina (average size 50 μm, density 3.89 g/cm^3) is provided by NICE Ltd India. E-glass fiber and polyester resin have a modulus of 72.5 and 3.25 GPa, respectively, and possess density of 2590 and 1350 kg/m^3, respectively. Composites of three different compositions (0, 10, and 20 wt% alumina filling) are made and the fiber-loading (weight fraction of glass fiber in the composite) is kept at 50% for all the samples. The castings are put under load for about 24 h for proper curing at room temperature. Specimens of suitable dimensions are cut using a diamond cutter for physical characterization and erosion testing.

Test Apparatus

Figure 1 shows the schematic diagram of an erosion test rig conforming to ASTM G 76. The set-up is capable of creating reproducible erosive situations for assessing erosion wear resistance of the prepared composite samples. It consists of an air compressor, an air

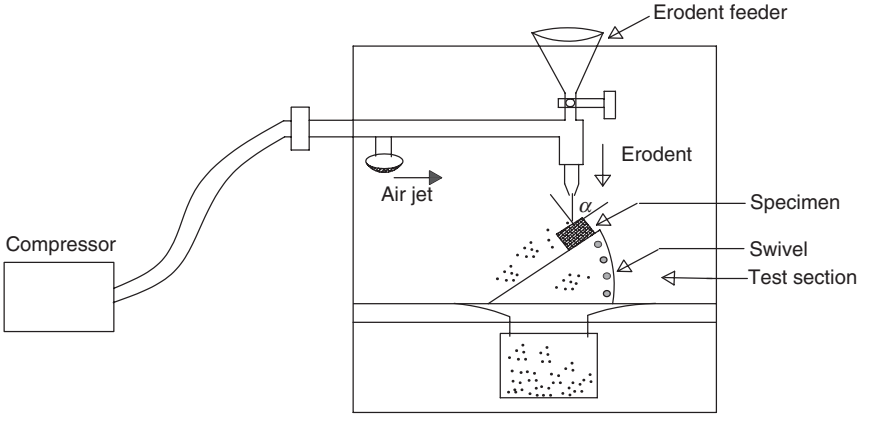

Figure 1. *A schematic diagram of the erosion test rig.*

particle mixing chamber, and accelerating chamber. Dry compressed air is mixed with the particles, which are fed at constant rate from a sand flow control knob through the nozzle tube and then accelerated by passing the mixture through a convergent brass nozzle of 3 mm internal diameter. These particles impact the specimen, which can be held at different angles with respect to the direction of erodent flow using a swivel and an adjustable sample clip. The velocity of the eroding particles is determined using a standard double-disc method [21]. In the present study, dry silica sand (spherical) of different particle sizes (30, 500, and 80 μm) are used as erodent. The samples are cleaned in acetone, dried, and weighed to an accuracy of ±0.1 mg before and after the erosion trials using a precision electronic balance. The weight loss is recorded for subsequent calculation of erosion rate. The process is repeated until the erosion rate attains a constant value, called the steady state erosion rate.

Test of Micro-hardness, Density, Tensile, and Flexural Properties

Micro-hardness measurement is done using a Leitz micro-hardness tester. A diamond indenter, in the form of a right pyramid with a square base and an angle 136° between opposite faces, is forced into the material under a load F. The two diagonals X and Y of the indentation left on the surface of the material after removal of the load are measured and their arithmetic mean L is calculated. In the present study, the load considered $F = 24.54$ N and Vickers hardness number is calculated using the equation:

$$H_V = 0.1889 \frac{F}{L^2} \tag{1}$$

and:

$$L = \frac{X + Y}{2}$$

where F is the applied load (N), L is the diagonal of square impression (mm), X is the horizontal length (mm), and Y is the vertical length (mm).

The tensile test is generally performed on flat specimens. The commonly used specimen for tensile test is the dog-bone specimen and straight-side specimen with end tabs. A uniaxial load is applied through both the ends. The ASTM standard test method for tensile properties of fiber resin composites has the designation D 3039-76. The length of the test section should be 200 mm. The tensile test is performed in the universal testing machine Instron 1195 and results are analyzed to calculate the tensile strength of composite samples.

The flexural strength of a composite is the maximum tensile stress that it can withstand during bending before reaching the breaking point. The three-point bend test is conducted on all the composite samples in the universal testing machine Instron 1195. Span length of 40 mm and the crosshead speed of 10 mm/min are maintained.

The surfaces of the specimens are examined directly by scanning electron microscope JEOL JSM-6480 LV. The eroded samples are mounted on stubs with silver paste. To enhance the conductivity of the eroded samples, a thin film of platinum is vacuum-evaporated onto them before the photomicrographs are taken.

Experimental Design

Design of experiment is a powerful analysis tool for modeling and analyzing the influence of control factors on performance output. The most important stage in the design of

Table 1. Levels of the variables used in the experiment.

	Level			
Control factor	**I**	**II**	**III**	**Units**
A: Velocity of impact	32	45	58	m/sec
B: Alumina percentage	0	10	20	%
C: Stand-off distance	120	180	240	mm
D: Impingement angle	45	60	90	degree
E: Erodent size	300	500	800	μm

Table 2. Orthogonal array for L_{27} (3^{13}) Taguchi design.

			3	4				8			11		
$L_{27}(3^{13})$	1 *A*	2 *B*	$(A \times B)_1$	$(A \times B)_2$	5 *C*	6	7	$(A \times C)_1$	9 *D*	10 *E*	$(A \times C)_2$	12	13
1	1	1	1	1	1	1	1	1	1	1	1	1	1
2	1	1	1	1	2	2	2	2	2	2	2	2	2
3	1	1	1	1	3	3	3	3	3	3	3	3	3
4	1	2	2	2	1	1	1	2	2	2	3	3	3
5	1	2	2	2	2	2	2	3	3	3	1	1	1
6	1	2	2	2	3	3	3	1	1	1	2	2	2
7	1	3	3	3	1	1	1	3	3	3	2	2	2
8	1	3	3	3	2	2	2	1	1	1	3	3	3
9	1	3	3	3	3	3	3	2	2	2	1	1	1
10	2	1	2	3	1	2	3	1	2	3	1	2	3
11	2	1	2	3	2	3	1	2	3	1	2	3	1
12	2	1	2	3	3	1	2	3	1	2	3	1	2
13	2	2	3	1	1	2	3	2	3	1	3	1	2
14	2	2	3	1	2	3	1	3	1	2	1	2	3
15	2	2	3	1	3	1	2	1	2	3	2	3	1
16	2	3	1	2	1	2	3	3	1	2	2	3	1
17	2	3	1	2	2	3	1	1	2	3	3	1	2
18	2	3	1	2	3	1	2	2	3	1	1	2	3
19	3	1	3	2	1	3	2	1	3	2	1	3	2
20	3	1	3	2	2	1	3	2	1	3	2	1	3
21	3	1	3	2	3	2	1	3	2	1	3	2	1
22	3	2	1	3	1	3	2	2	1	3	3	2	1
23	3	2	1	3	2	1	3	3	2	1	1	3	2
24	3	2	1	3	3	2	1	1	3	2	2	1	3
25	3	3	2	1	1	3	2	3	2	1	2	1	3
26	3	3	2	1	2	1	3	1	3	2	3	2	1
27	3	3	2	1	3	2	1	2	1	3	1	3	2

experiment lies in the selection of the control factors. Therefore, a large number of factors are included so that non-significant variables can be identified at the earliest opportunity. Exhaustive literature review on erosion behavior of polymer composites reveals that parameters, viz., impact velocity, impingement angle, fiber-loading, filler content, erodent size, and stand-off distance, etc., largely influence the erosion rate of polymer composites [22,23]. The impact of five such parameters are studied using L_{27} (3^{13}) orthogonal design. The operating conditions under which erosion tests are carried out are given in Table 1. The tests are conducted as per experimental design given in Table 2 at room temperature.

In Table 2, each column represents a test parameter whereas a row stands for a treatment or test condition which is nothing but a combination of parameter levels.

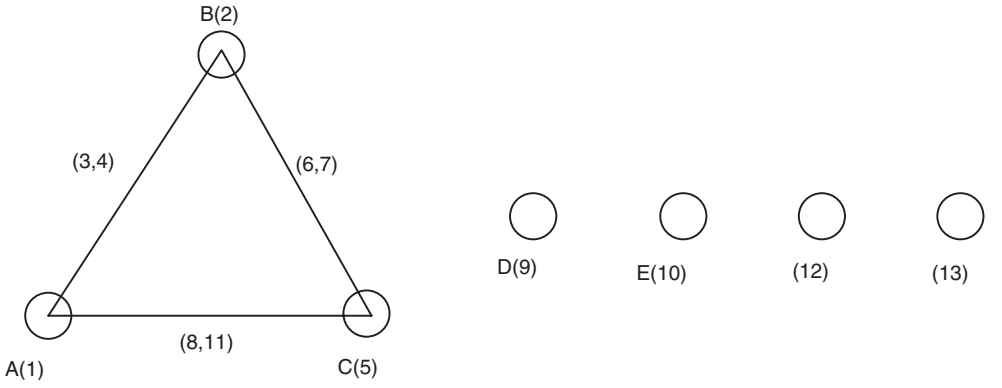

Figure 2. *Linear graphs for L_{27} array.*

In conventional full factorial experiment design, it would require $3^5 = 243$ runs to study five parameters each at three levels, whereas Taguchi's factorial experiment approach reduces it to only 27 runs, offering a great advantage in terms of experimental time and cost. The experimental observations are further transformed into signal-to-noise (S/N) ratio. There are several S/N ratios available depending on the type of performance characteristics. The S/N ratio for minimum erosion rate can be expressed as a 'lower is better' characteristic, which is calculated as logarithmic transformation of loss function as shown below:

$$\text{Lower is better characteristic:} \quad \frac{S}{N} = -10\log\frac{1}{n}\left(\sum y^2\right) \tag{2}$$

where 'n' is the number of observations and y is the observed data. The standard linear graph, as shown in Figure 2, is used to assign the factors and interactions to various columns of the orthogonal array [24].

The plan of the experiments is as follows: the first column is assigned to impact velocity (A), the second column to alumina percentage (B), the fifth column to stand-off distance (C), the ninth column to impingement angle (D), and the tenth column to erodent size (E). The third and fourth column are assigned to $(A \times B)_1$ and $(A \times B)_2$, respectively, to estimate interaction between impact velocity (A) and alumina percentage (B), the eighth and eleventh columns are assigned to $(A \times C)_1$ and $(A \times C)_2$, respectively, to estimate interaction between the impact velocity (A), and stand-off distance (C), and the remaining columns are used to estimate experimental errors.

RESULTS AND DISCUSSION

Mechanical Properties

In the present investigation the addition of alumina filler in glass polyester hybrid composite has not shown encouraging results in terms of mechanical properties. Figure 3(a) and (b) present the tensile strengths and tensile moduli of the composites with and without filler. It can be seen that the tensile properties have become distinctly poorer with the incorporation of alumina particles in the matrix. Previous reports [25,26] demonstrate that normally the glass fibers in the composite restrain the deformation of the

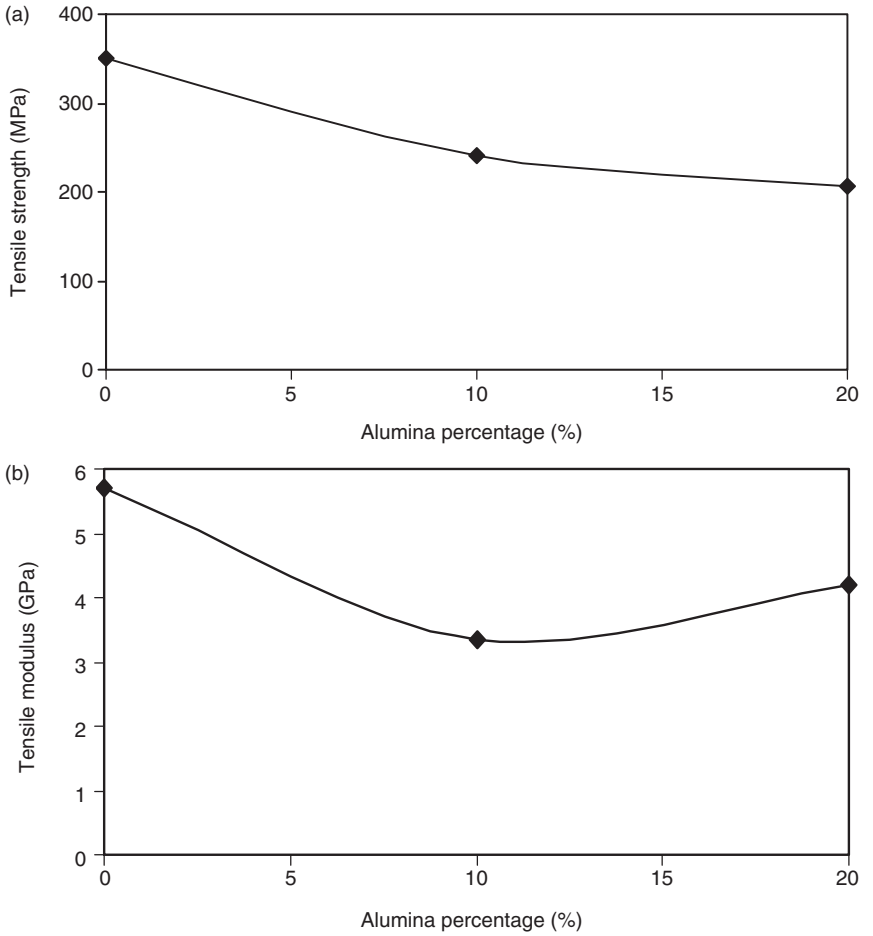

Figure 3. *(a) Effect of alumina filling on tensile strength of the hybrid composite; (b) effect of alumina filling on tensile modulus of the hybrid composite.*

matrix polymer, reducing the tensile strain. So even if the strength decreases with filler addition, the tensile modulus of the hybrid composite is expected to increase. However, this is possibly not occurring in the present case with the presence of alumina as the filler and, as a result, reduction in both tensile strength and modulus is recorded in spite of the reinforcement of long glass fibers. Moreover, alumina affecting the crystalline structure of semi-crystalline thermoplastic polyester may be another reason for the deteoriation of tensile properties. This might have influenced the flexural strength of these hybrid composites, which is showing (Figure 4) a decreasing trend beyond a filler content of 10 wt%.

The micro-hardness of the glass polyester composite is not seen to significantly change with the addition of alumina (Figure 5). However the density of the composites has reduced with alumina filling. The neat polyester taken for this study possess a density of 1.35 g/cm^3 which increases to 1.93 g/cm^3 with the reinforcement of 50 wt% of glass fiber in it. But when the matrix is filled with micro-sized alumina particles, the density of the resulting hybrid composite reduces, and this reduction is almost proportional to the filler content (Figure 6).

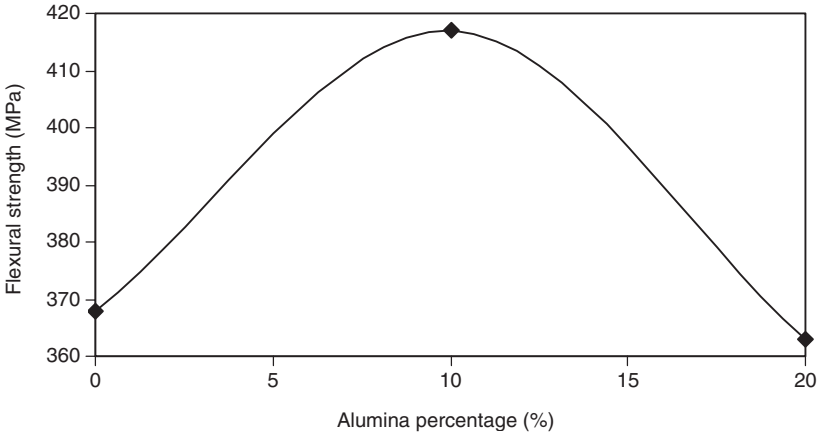

Figure 4. *Effect of alumina filling on flexural strength of the hybrid composites.*

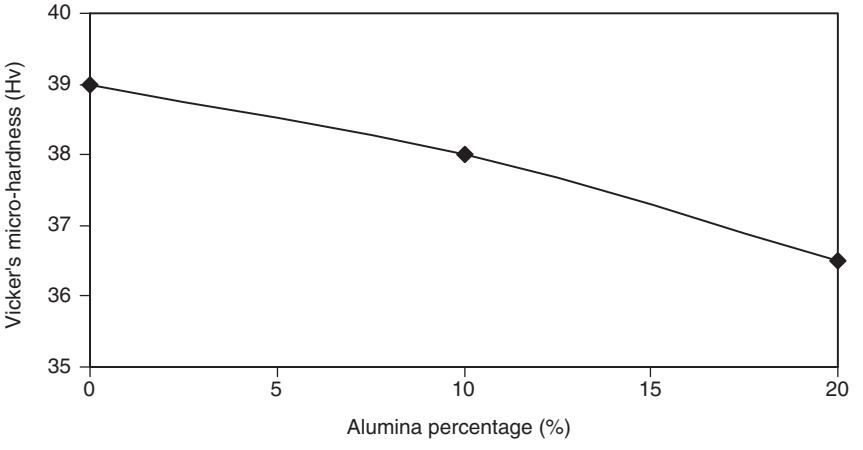

Figure 5. *Variation of Vicker's micro-hardness with alumina percentage.*

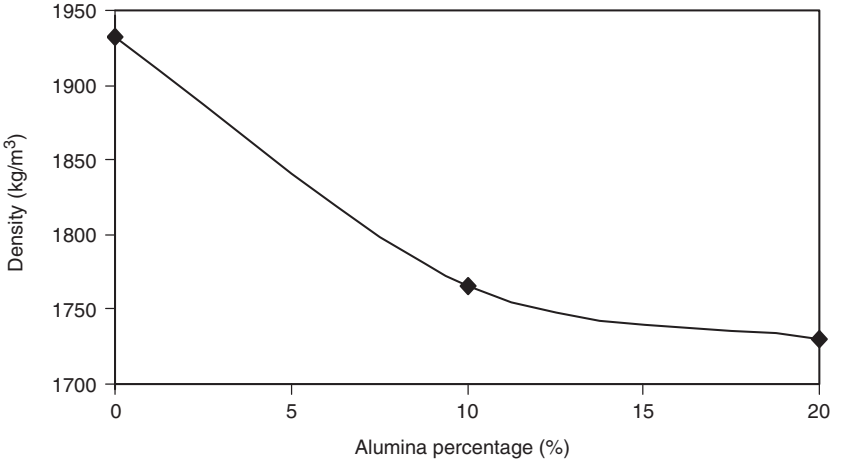

Figure 6. *Effect of alumina filling on density of the hybrid composite.*

Surface Morphology

Figure 7(a) shows a portion of the composite surface before erosion occurred. Scattered alumina particles are observed on the upper surface. The distribution of filler as seen in the micrograph is reasonably uniform, although in places the particles are seen to have formed small and big clusters. Figure 7(b) shows the micrograph of surface eroded at an impingement angle of 60° and an impact velocity of 45 m/s. A small portion of a fiber exposed during the sand erosion is noticed. The matrix covering the fiber seems to be chipped off and the crater thus formed shows the fiber body, which is almost intact. Repeated impact of the erodent has caused roughening of the surface. Erosion along the fibers and clean removal of the matrix at the interface is observed in the magnified image given alongside. Figure 7(c) clearly shows the crater formation due to penetration of hard silica sand particles onto the surface, causing material removal mostly from the matrix regime. Small cracks and multiple fractures are also distinctly shown in this micrograph.

Particle impingement produces a rise in the temperature of the surface, which makes the matrix deformation easy because the high temperature known to occur in solid particle erosion invariably softens the matrix [27]. On impact, the erodent particle kinetic energy is transferred to the composite body which leads to crater formation and subsequently material loss. The presence of hard alumina particle in the matrix helps in absorbing a good fraction of this kinetic energy and therefore energy available for the plastic deformation of thermoplastic polyester becomes less. This also delays the initiation of fiber exposure as compared to the composite without any filler. All these factors combined together result in exhibition of better erosion response by the alumina-filled composites than that of fiber-reinforced polyester without particulate filling.

Steady State Erosion

Thermoplastic matrix composites usually show ductile erosion, while the thermosetting ones erode in a brittle manner. Thus the erosion wear behavior of polymer composites can be grouped into ductile and brittle categories, although this grouping is not definitive because the erosion characteristics depend equally on the experimental conditions as on composition of the target material. It is well known that impingement angle is one of the most important parameters in the erosion process, and for ductile materials the peak erosion occurs at 15° to 20° angle while for brittle materials the erosion damage is maximum usually at normal impact, i.e., 90° angle. In the present study the variation of erosion wear rate of the hybrid composites with impingement angle under similar operating conditions is investigated. The result is presented in Figure 8, which shows the peak erosion taking place at an impact angle of 60°. This clearly indicates that these hybrid composites respond to solid particle erosion in neither a purely ductile nor a purely brittle manner. This behavior can be termed as semi-ductile in nature. The loss of ductility may be attributed to the incorporation of glass fibers and alumina particles, both of which are brittle.

In Table 3, the last column represents S/N ratio of the erosion rate, which is in fact the average of two replications. The overall mean for the S/N ratio of the erosion rate is found to be −46.33 dB. The analysis was made using the popular software, specifically used for design of experiment applications, known as MINITAB 14. Before any attempt is made to use this simple model as a predictor for the measure of performance, the possible interactions between the control factors must be considered. Thus factorial design incorporates a simple means of testing for the presence of the interaction effects.

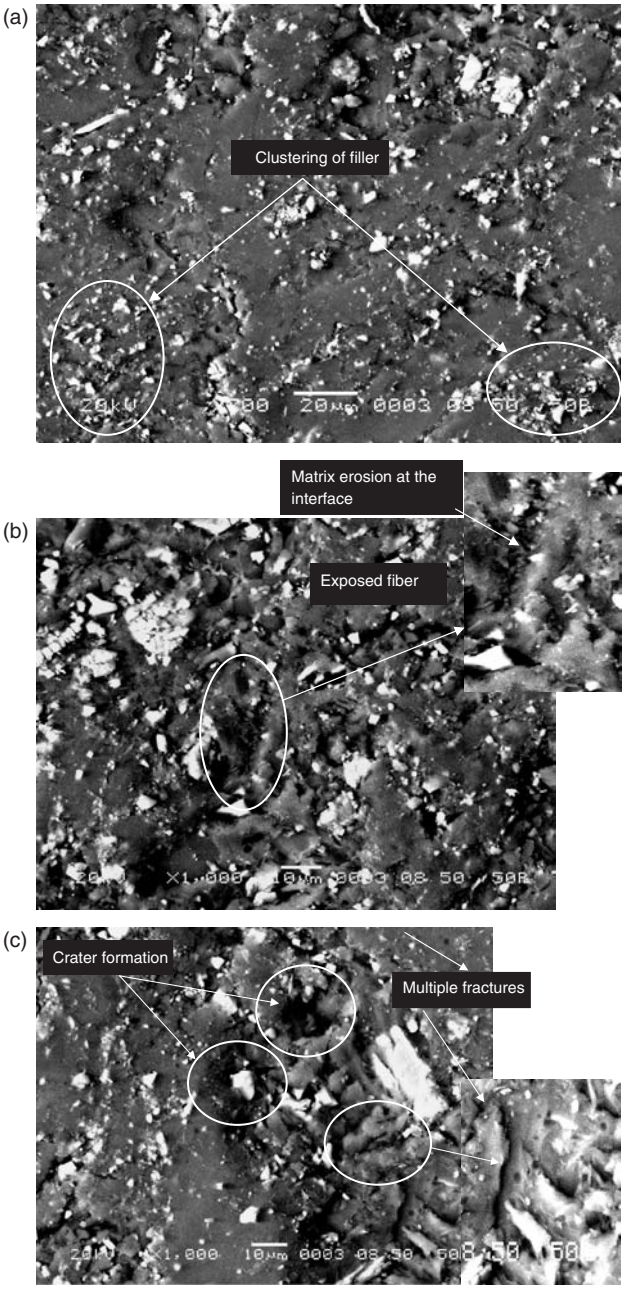

Figure 7. *(a) Scanning electron micrograph of uneroded composite surface (alumina content 20%); (b) scanning electron micrograph of eroded composite surface (impact velocity 45 m/s, alumina content 20%, S.O.D 180 mm, impingement angle 60°, and erodent size 80 μm); (c) scanning electron micrograph of eroded composite surface (impact velocity 58 m/s, alumina content 20%, S.O.D. 180 mm, impingement angle 60°, and erodent size 80 μm).*

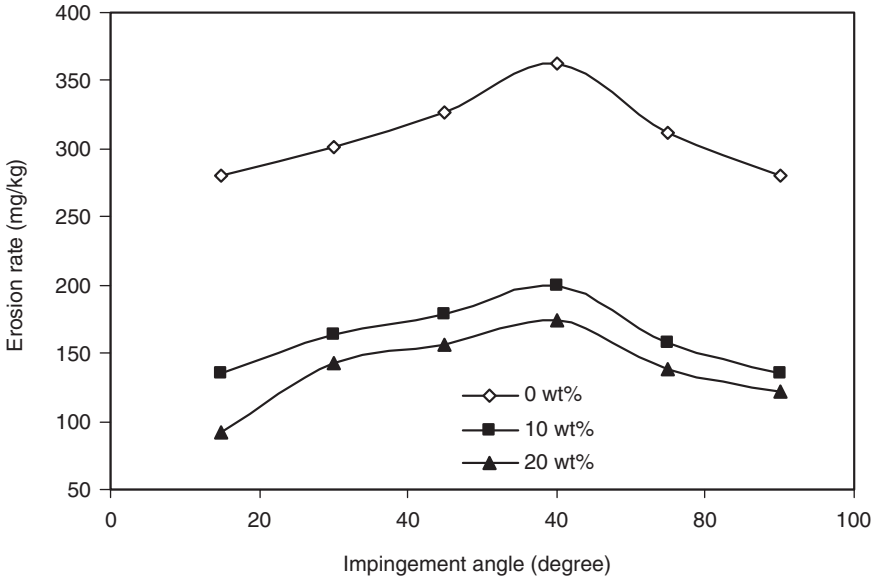

Figure 8. *Erosion rate vs angle of impingement for different alumina filling.*

Analysis of the result leads to the conclusion that factor combination of A_1, B_2, C_3, D_1, and E_2 gives minimum erosion rate. This is evident from Figure 9. As far as minimization of erosion rate is concerned, factors A, B, D, and E have significant effect whereas factor C has least effect. It is observed from Figure 10 that the interaction between $A \times B$ shows the most significant effect on erosion rate. From this analysis we concluded that few of the factors have an individual effect on the erosion rate and similarly, few of the interactions have a combined effect on erosion rate.

Erosion Efficiency

The hardness alone is unable to provide sufficient correlation with erosion rate, largely because it determines only the volume displaced by each impact and not really the volume eroded. Thus, a parameter which will reflect the efficiency with which the volume displaced is removed should be combined with hardness to obtain a better correlation. The erosion efficiency is obviously one such parameter. In the case of a stream of particles impacting a surface normally (i.e., at $\alpha = 90^\circ$), erosion efficiency (η_{normal}) defined by Sundararajan et al. [28] is given as:

$$\eta_{\text{normal}} = \frac{2ErHv}{\rho V^2}. \tag{3a}$$

However, considering impact of erodent at any angle α to the surface, the actual erosion efficiency (η) can be obtained by modifying Equation (3a) as:

$$\eta = \frac{2ErHv}{\rho V^2 \sin^2 \alpha}. \tag{3b}$$

Table 3. Experimental design using L_{27} orthogonal array.

Expt. No.	Impact velocity (*A*) m/s	Alumina percentage (*B*) %	Stand-off distance (*C*) mm	Impingement angle (*D*) degree	Erodent size (*E*) μm	Erosion rate (*Er*) mg/kg	*S*/*N* ratio (db)
1	32	0	120	30	300	309.83	−49.8225
2	32	0	180	60	500	235.25	−47.4306
3	32	0	240	90	800	315.19	−49.9714
4	32	10	120	60	500	173.77	−44.7995
5	32	10	180	90	800	264.94	−48.4630
6	32	10	240	30	300	139.96	−42.9201
7	32	20	120	90	800	289.48	−49.2324
8	32	20	180	30	300	227.49	−47.1392
9	32	20	240	60	500	197.88	−45.9280
10	45	0	120	60	800	318.86	−50.0720
11	45	0	180	90	300	349.80	−50.8764
12	45	0	240	30	500	235.25	−47.4306
13	45	10	120	90	300	174.94	−44.8578
14	45	10	180	30	500	133.18	−42.4888
15	45	10	240	60	800	172.78	−44.7499
16	45	20	120	30	500	183.96	−45.2945
17	45	20	180	60	800	287.83	−49.1827
18	45	20	240	90	300	311.76	−49.8764
19	58	0	120	90	500	395.10	−51.9341
20	58	0	180	30	800	215.19	−46.6564
21	58	0	240	60	300	239.89	−47.6002
22	58	10	120	30	800	207.34	−46.7428
23	58	10	180	60	300	259.79	−48.2924
24	58	10	240	90	500	184.44	−45.3171
25	58	20	120	60	300	282.68	−49.0259
26	58	20	180	90	500	318.96	−50.0747
27	58	20	240	30	800	305.88	−49.7110

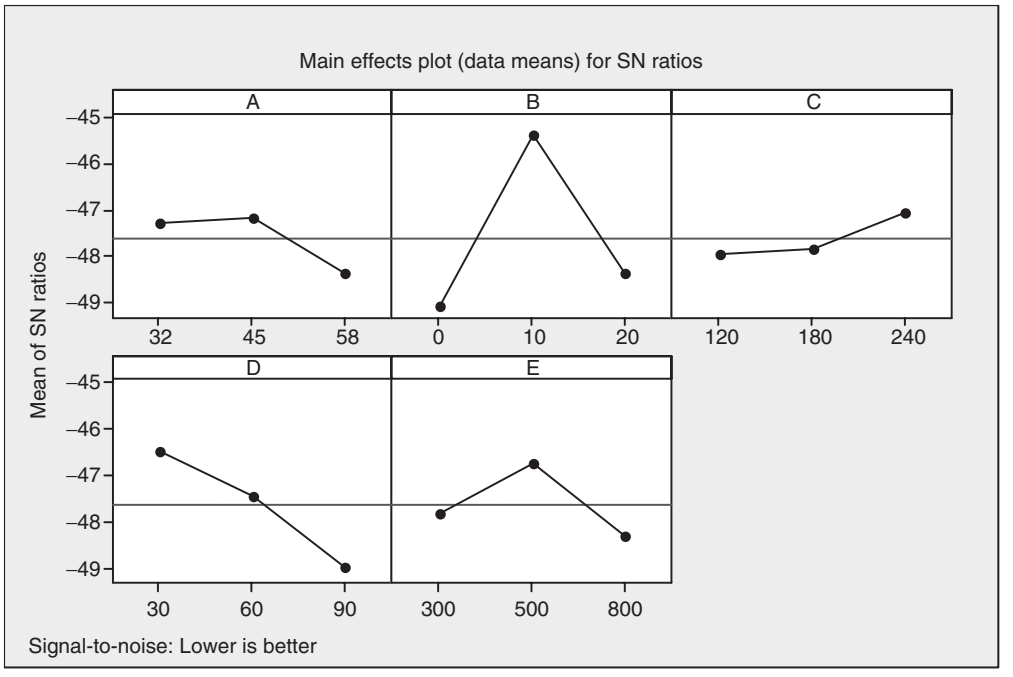

Figure 9. *Effect of control factors on erosion rate.*

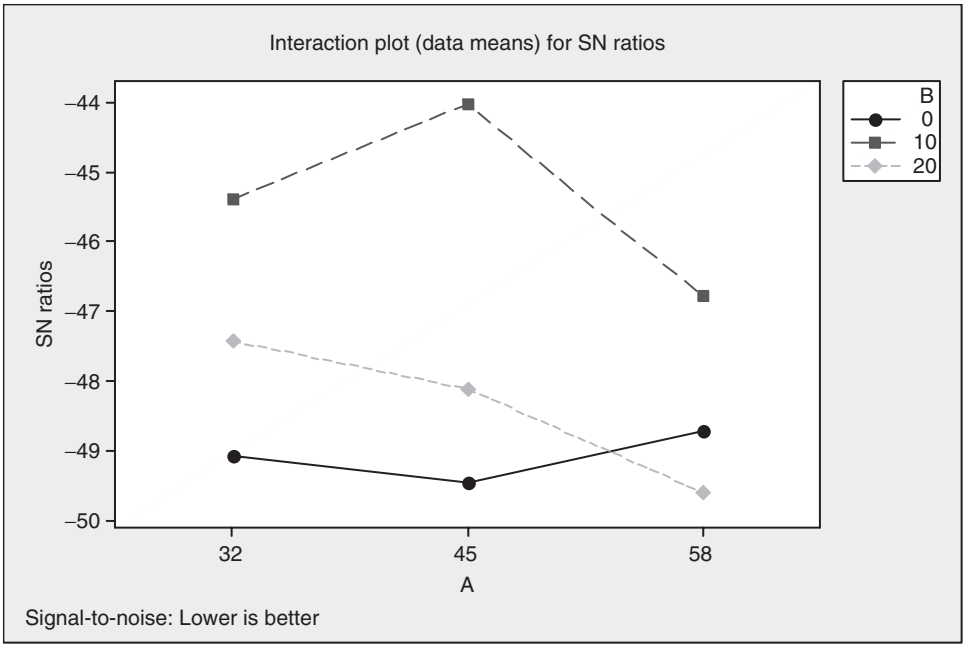

Figure 10. *Interaction graph between A × C for erosion rate.*

Table 4. Erosion efficiency for different alumina percentage.

Expt. No.	Alumina percentage (%)	Impact velocity (*V*) m/s	Density of target material (ρ) kg/m^3	Hardness of target material (*Hv*) MPa	Erosion rate (*Er*) mg/kg	Erosion efficiency (η)%
1	0	32	1932	39	309.83	47.91894
2	0	32	1932	39	235.25	10.49685
3	0	32	1932	39	315.19	12.18698
4	10	32	1765	38	173.77	8.26962
5	10	32	1765	38	264.94	10.92578
6	10	32	1765	38	139.96	23.08708
7	20	32	1730	36.5	289.48	11.69854
8	20	32	1730	36.5	227.49	36.77353
9	20	32	1730	36.5	197.88	9.228278
10	0	45	1932	39	318.86	7.194564
11	0	45	1932	39	349.80	6.839407
12	0	45	1932	39	235.25	18.39875
13	10	45	1765	38	174.94	3.648120
14	10	45	1765	38	133.18	11.10910
15	10	45	1765	38	172.78	4.157950
16	20	45	1730	36.5	183.96	15.03735
17	20	45	1730	36.5	287.83	6.787811
18	20	45	1730	36.5	311.76	6.371010
19	0	58	1932	39	395.10	4.650233
20	0	58	1932	39	215.19	10.13094
21	0	58	1932	39	239.89	3.258259
22	10	58	1765	38	207.34	10.41099
23	10	58	1765	38	259.79	3.763373
24	10	58	1765	38	184.44	2.315284
25	20	58	1730	36.5	282.68	4.012895
26	20	58	1730	36.5	318.96	3.923676
27	20	58	1730	36.5	305.88	15.05109

where E_r is the erosion rate (kg/kg), H_v is the hardness of target material (Pa), ρ is the density of the erodent (kg/m^3), and V is the impact velocity (m/s).

The values of erosion efficiencies of these composites calculated using Equation (3b) are summarized in Table 4 along with their hardness values and operating conditions. The table clearly shows that erosion efficiency is not exclusively a material property, but also depends on other operational variables such as impingement angle and impact velocity. The erosion efficiencies of these composites under normal impact (η_{normal}) vary from 3–6%, 6–9%, and 9–12% for impact velocities 58, 45, and 32 m/s, respectively. The value of η for a particular impact velocity under oblique impact can be obtained simply by multiplying a factor $1/\sin^2\alpha$ with $\eta_{\text{normal.}}$ Similar observation on velocity dependence of erosion efficiency has previously been reported by some investigators [22,23].

The magnitude of η can be used to characterize the nature and mechanism of erosion. For example, ideal micro-ploughing involving just the displacement of the material from the crater without any fracture (and hence no erosion) will result in $\eta = 0$. In contrast, if the material removal is by ideal micro-cutting, $\eta = 1.0$ or 100%. If erosion occurs by lip or platelet formation and their fracture by repeated impact, as is usual in the case of ductile materials, the magnitude of η will be very low, i.e. $\eta \leq 100\%$. In the case of brittle materials, erosion occurs usually by spalling and removal of large chunks of materials

Table 5. ANOVA table for erosion rate.

Source	DF	Seq SS	Adj SS	Adj MS	F	P
A	2	7.580	7.580	3.790	1.62	0.256
B	2	68.885	68.885	34.442	14.75	0.002
C	2	4.455	4.455	2.228	0.95	0.425
D	2	28.269	28.269	14.134	6.05	0.025
E	2	11.548	11.548	5.774	2.47	0.146
$A \times B$	4	11.968	11.968	2.992	1.28	0.354
$A \times C$	4	5.705	5.705	1.426	0.61	0.667
Error	8	18.685	18.685	2.336		
Total	26	157.095				

resulting from the interlinking of lateral or radial cracks and thus η can be expected to be even greater than 100% [22]. The erosion efficiencies of the composites under the present study indicate that at low impact speed the erosion response is semi-ductile ($\eta = 10$–100%). On the other hand, at relatively higher impact velocity the composites exhibit ductile ($\eta < 10\%$) erosion behavior [29].

ANOVA and the Effects of Factors

In order to find out the statistical significance of various factors like impact velocity (A), alumina percentage (B), stand-off distance (C), impingement angle (D), and erodent size (E) on erosion rate, analysis of variance (ANOVA) is performed on the experimental data. Table 5 shows the results of the ANOVA with the erosion rate. This analysis is undertaken for a level of confidence of significance of 5%. The last column of the table indicates that the main effects are highly significant (all have very small p-values).

From Table 5, one can observe that alumina percentage ($p = 0.002$), impingement angle ($p = 0.025$), erodent size ($p = 0.146$) and impact velocity ($p = 0.256$) have great influence on erosion rate. The interaction of impact velocity $\times$ alumina percentage ($p = 0.354$) shows significant contribution to the erosion rate but the remaining factors and interactions have relatively less significant contribution to erosion rate.

CONFIRMATION EXPERIMENT

The optimal combination of control factors has been determined in the previous analysis. However, the final step in any design of experiment approach is to predict and verify improvements in observed values through the use of the optimal combination level of control factors. The confirmation experiment is performed by taking an arbitrary set of factor combination $A_1B_3D_2E_3$; factor C has been omitted because factor C and interaction $A \times C$ have the least effect on erosion rate, as evident from Table 5. The estimated S/N ratio for erosion rate can be calculated with the help of following prediction equation:

$$\hat{\eta}_1 = \bar{T} + (\bar{A}_1 - \bar{T}) + (\bar{B}_3 - \bar{T}) + [(\bar{A}_1\bar{B}_3 - \bar{T}) - (\bar{A}_1 - \bar{T}) - (\bar{B}_3 - \bar{T})] + (\bar{D}_2 - \bar{T}) + \left(\bar{E}_3 - \bar{T}\right) \tag{4}$$

Table 6. Results of the confirmation experiments for erosion rate.

	Optimal control parameters	
	Prediction	**Experimental**
Level	$A_1B_3D_2E_3$	$A_1B_3D_2E_3$
S/N ratio for erosion rate (mg/kg)	−47.9446	−45.6864

where $\bar{\eta}_1$ is the predicted average, $\bar{T}$ is the overall experimental average, and $\bar{A}_1, \bar{B}_3, \bar{D}_2$, and $\bar{E}_3$ are mean responses for factors and interactions at designated levels.

By combining like terms, the equation reduces to:

$$\bar{\eta}_1 = \bar{A}_1\bar{B}_3 + \bar{D}_2 + \bar{E}_3 - 2\bar{T}. \tag{5}$$

A new combination of factor levels A_1, B_3, D_1 and E_3 is used to predict deposition rate through prediction equation, and it is found to be $\bar{\eta}_1 = -47.9446$ dB.

For each performance measure, an experiment is conducted for a different factor combination and compared with the result obtained from the predictive equation as shown in Table 6.

The resulting model seems to be capable of predicting erosion rate to a reasonable accuracy. An error of 4.71% for the S/N ratio of erosion rate is observed. However, the error can be further reduced if the number of measurements is increased. This validates the development of the mathematical model for predicting the measures of performance based on knowledge of the input parameters.

FACTOR SETTINGS FOR MINIMUM EROSION RATE

In this study, an attempt is made to derive optimal settings of the control factors for minimization of erosion rate. The single-objective optimization requires quantitative determination of the relationship between erosion rates with a combination of control factors. In order to express the erosion rate in terms of a mathematical model, the following form is suggested:

$$Er = K_0 + K_1 \times A + K_2 \times B + K_3 \times D + K_4 \times E + K_5 \times A \times B. \tag{6}$$

Here, Er is the performance output terms and K_i ($i = 0, 1, \ldots, 5$) are the model constants. The constants are calculated using non-linear regression analysis with the help of SYSTAT 7 software, and the following relations are obtained:

$$\begin{aligned} Y &= 0.467 - 0.031 \times A - 0.355 \times B + 0.273 \times D + 0.053 \times E + 0.382 \times A \times B \\ r^2 &= 0.95. \end{aligned} \tag{7}$$

The correctness of the calculated constants is confirmed as high correlation coefficients (r^2) to the value of 0.95 obtained for Equation (6) and, therefore, the models are quite suitable to use for further analysis. Here, the resultant objective function to be maximized is given as:

$$\text{Maximize } Z = \frac{1}{f} \tag{8}$$

Table 7. Optimum conditions for performance output.

Control factors and performance characteristics	Optimum conditions
A: Impact velocity (m/s)	56.89
B: Alumina percentage (%)	11.82
D: Impingement angle (degree)	61.56
E: Erodent size (μm)	788.0
Erosion rate (mg/kg)	271.83

where f is the normalized function for erosion rate subjected to constraints:

$$A_{\min} \leq A \leq A_{\max} \tag{9}$$

$$B_{\min} \leq B \leq B_{\max} \tag{10}$$

$$D_{\min} \leq D \leq D_{\max} \tag{11}$$

$$E_{\min} \leq E \leq E_{\max}. \tag{12}$$

The min and max in Equations (9)–(12) show the lowest and highest control factor settings (control factors) used in this study (Table 1).

A genetic algorithm (GA) is used to obtain the optimum value for single-objective outputs to optimize the single-objective function. The technique has been successfully implemented earlier for determining the optimal factor settings in case of erosion wear of flyash-filled glass-polyester composite, and also effectively conducted without addition of filler material in the glass-polyester composite [30,31]. The computational algorithm is implemented in Turbo C^{++} and run on an IBM Pentium IV machine. Genetic algorithms (GAs) are mathematical optimization techniques that simulate a natural evolution process. They are based on the Darwinian theory, in which the fittest species survive and propagate while the less successful tend to disappear. The genetic algorithm mainly depends on three types of operators, viz., reproduction, crossover, and mutation. Reproduction is accomplished by copying the best individuals from one generation to the next, which is often called an elitist strategy. The best solution is monotonically improving from one generation to the next. The selected parents are submitted to the crossover operator to produce one or two children. The crossover is carried out with an assigned probability, which is generally rather high. If a number, randomly sampled, is inferior to the probability, the crossover is performed. The genetic mutation introduces diversity in the population by an occasional random replacement of the individuals. The mutation is performed based on an assigned probability. A random number is used to determine if a new individual will be produced to substitute the one generated by crossover. The mutation procedure consists of replacing one of the decision variable values of an individual while keeping the remaining variables unchanged. The replaced variable is randomly chosen and its new value is calculated by randomly sampling within its specific range. In genetic optimization, population size, probability of crossover, and mutation are set at 50, 75, and 5%, respectively, for all the cases. The number of generations is varied until the output is converted. Table 7 shows the optimum conditions of the control factors with optimum performance output giving a better combination of set of

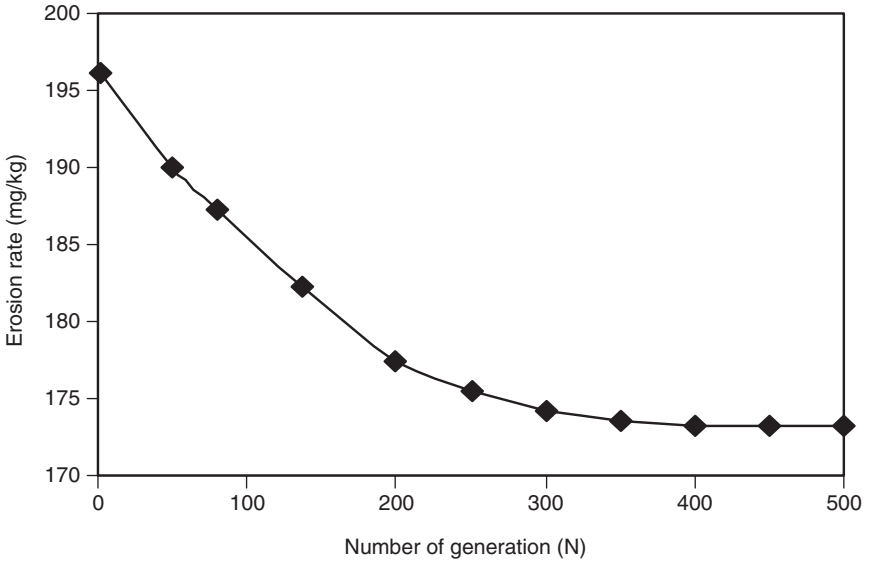

Figure 11. *Convergence curve.*

input control factors. The pattern of convergence of performance output with number of generations is shown in Figure 11.

CONCLUSIONS

This analytical and experimental investigation into the erosion behavior of alumina-GF-polyester hybrid composites leads to the following conclusions:

Hybrid composites suitable for applications in highly erosive environments can be prepared by reinforcement of glass fibers and filling of micro-sized alumina particles in thermoplastic polyester resin. The erosion wear performance of these composites improves quite significantly by addition of alumina filler. On the other hand, due to the presence of these particulates, the composite suffers a loss in tensile as well as flexural strength.

Erosion characteristics of these composites can be successfully analyzed using the Taguchi experimental design scheme. Taguchi method provides a simple, systematic, and efficient methodology for the optimization of the control factors.

The erosion efficiency (η), in general, characterizes the wear mechanism of composites. The alumina-filled GF-polyester composites exhibit semi-ductile erosion response ($\eta = 10$–60%) for low impact velocities and ductile erosion response ($\eta < 10\%$) for relatively high impact velocity.

Factors like alumina percentage, impingement angle, erodent size, and impact velocity, in order of priority, are significant to minimize the erosion rate. Although the effect of impact velocity is less compared to other factors, it cannot be ignored because it shows significant interaction with another factor, i.e. the percentage of alumina in the composite.

Study of influence of impingement angle on erosion rate of the composites filled with different percentages of alumina reveals their semi-ductile nature with respect to erosion wear. The peak erosion rate is found to be occurring at 60° impingement angle under various experimental conditions.

The rationale behind the use of genetic algorithm lies in the fact that genetic algorithm has the capability to find the global optimal parameter settings whereas the traditional optimization techniques are normally stuck at the local optimum values. The optimum settings are found to be impact velocity = 56.89 m/s, alumina percentage = 11.82%, impingement angle = 61.56°, erodent size = 78 μm, and resulting erosion rate = 271.83 mg/kg as far as present experimental conditions are concerned.

In future, this study can be extended to new hybrid composites using other potential fillers and the resulting experimental findings can be similarly analyzed.

REFERENCES

1. Gregory, S. W., Freudenberg, K. D., Bhimaraj, P. and Schadler, L. S. (2003). A Study on the Friction and Wear Behavior of PTFE Filled With *Alumina Nanoparticles*, *Wear,* **254**: 573–580.
2. Jung-il, K., Kang, P. H. and Nho, Y. C. (2004). Positive Temperature Coefficient Behavior of Polymer Composites Having a High Melting Temperature, *J. Appl. Polym. Sci.*, **92**: 394–401.
3. Nikkeshi, S., Kudo, M. and Masuko, T. (1998). Dynamic Viscoelastic Properties and Thermal Properties of Powder-Epoxy Resin Composites, *J. Appl. Poly. Sci.*, **69**: 2593–2598.
4. Zhu, K. and Schmauder, S. (2003). Prediction of the Failure Properties of Short Fiber Reinforced Composites With Metal and Polymer Matrix, *Comput. Mater. Sci.*, **28**: 743–748.
5. Rusu, M., Sofian, N. and Rusu, D. (2001). Mechanical and Thermal Properties of Zinc Powder Filled High Density Polyethylene Composites, *Polym. Test*., **20**: 409–417.
6. Tavman, I. H. (1997). Thermal and Mechanical Properties of Copper Powder Filled Poly(ethylene) Composites, *Powder Technol*., **91**: 63–67.
7. Rothon, R. N. (1999). Mineral Fillers in Thermoplastics: Filler Manufacture and Characterization, *Adv. Polym. Sci*., **139**: 67–107.
8. Rothon, R. N. (1997). Mineral Fillers in Thermoplastics: Filler Manufacture, *J Adhesion*, **64**: 87–109.
9. Cirino, M., Pipes, R. B. and Friedrich, K. (1987). The Abrasive Wear Behaviour of Continuous Fibre Polymer Composites, *J. Mater. Sci*., **22**: 2481–2492.
10. Cirino, M., Friedrich, K. and Pipes, R. B. (1988). Evaluation of Polymer Composites for Sliding and Abrasive Wear Application, *Composites*, **19**: 383–392.
11. Lhymn, C., Tempelmeyer, K. E. and Davis, P. K. (1985). The Abrasive Wear of Short Fibre Composites, *Composites*, **16**: 127–136.
12. Voss, H. and Friedrich, K. (1987). On the Wear Behaviour of Short Fibre Reinforced PEEK Composites, *Wear*, **116**: 1–18.
13. Briscoe, B. J., Yao, L. H. and Stolarski, T. A. (1986). The Friction and Wear of PTFE and PEEK Composites: An Initial Appraisal of the Optimum Composition, *Wear*, **108**: 357–368.
14. Friedrich, K., Lu, Z. and Hager, A. M. (1993). Overview on Polymer Composites for Friction and Wear Application, *J. Theor. Appl. Fract. Mech*., **19**: 1–11.
15. Bahadur, S. and Gong, D. (1992). The Role of Copper Compounds as Fillers in the Transfer and Wear Behaviour of PEEK, *Wear*, **154**: 151–165.
16. Wang, Q. H., Xue, Q. J., Shen, W. C. and Zhang, J. (1998). The Friction and Wear Properties of Nanometer ZrO_2-Filled PEEK, *J. Appl. Polym. Sci*., **69**: 135–141.
17. Wang, Q. H., Xue, Q. J. and Shen, W. C. (1998). The Tribological Properties of SiC Whisker Reinforced PEEK, *J. Appl. Polym. Sci*., **69**: 2341–2347.
18. Wang, Q. H., Xue, Q. J., Liu, W. M. and Chen, J.-M. (2000). The Friction and Wear Characteristics of Nanometer SiC and PTFE Filled PEEK, *Wear*, **243**: 140–146.
19. Voss, H. and Friedrich, K. (1986). Wear Performance of Bulk Liquid Crystal Polymer and its Short Fibre Composites, *Tribol. Int*., **19**: 145–156.
20. Harsha, A. P. and Tewari, U. S. (2002). Tribo Performance of Polyaryletherketone Composites, *Polymer Testing*, **21**: 697–709.
21. Aglan, H. A. and Chenock Jr, T. A. (1993). Erosion Damage Features of Polyimide Thermoset Composites, *SAMPEQ*, pp. 41–47.
22. Srivastava, V. K. and Pawar, A. G. (2006). Solid Particle Erosion of Glass Fiber Reinforced Flyash Filled Epoxy Resin Composites, *Composite Science and Technology*, **66**: 3021–3028.

23. Suresh, A. and Harsha, A. P. (2006). Study of Erosion Efficiency of Polymers and Polymer Composites, *Polymer Testing*, **25**: 188–196.
24. Glen, S. P. (1993). *Taguchi Methods: A Hands on Approach*, Addison-Wesley, New York.
25. Fu, S.-Y. and Lauke, B. (1998). Characterization of Tensile Behavior of Hybrid Short Glass Fiber/Calcite Particles/ABS Composites, *Composites: Part A*, **29**: 575–583.
26. Thomason, J. L., Vlug, M. A., Schipper, G. and Krikor, HGLT. (1996). Influence of Fibre Length and Concentration on the Properties of Glass Fibre Reinforced Polypropylene: Part 3. Strength and Strain at Failure, *Composites: Part A*, **27**: 1075–1084.
27. Tewari, U. S., Harsha, A. P., Hager, A. M. and Friedrick, K. (2002). Solid Particle Erosion of Unidirectional Carbon Fiber Reinforced Polyetheretherketone Composites, *Wear*, **252**: 992–1000.
28. Sundararajan, G., Roy, M. and Venkataraman, B. (1990). Erosion Efficiency – A New Parameter to Characterize the Dominant Erosion Micromechanism, *Wear*, **140**: 369–381.
29. Roy, M., Vishwanathan, B. and Sundararajan. G. (1994). The Solid Particle Erosion of Polymer Matrix Composites, *Wear*, **171**: 149–161.
30. Amar, P., Alok, S., Mahapatra, S. S. and Dash, R. R. (2007). Modeling and Prediction of Erosion Response of Glass Reinforced Polyester–Flyash Composites, *Journal of Reinforced Plastics and Composites*. (In press).
31. Amar, P., Alok, S., Mahapatra, S. S. and Dash, R. R. (2007). A Taguchi Approach for Investigation of Erosion of Glass Fiber–Polyester Composites, *Journal of Reinforced Plastics and Composites* (In Press).